

Terdiurnal signatures in midlatitude sporadic E layers occurrence rates

T. Fytterer, C. Arras, and C. Jacobi

Summary

Global Positioning System radio occultation measurements by the FORMOSA SATellite mission-3/Constellation Observing System for Meteorology, Ionosphere and Climate satellites were used to analyse the behaviour of the signature of the terdiurnal tide in sporadic E (E_s) layers at midlatitudes ($43^\circ\text{N} - 63^\circ\text{N}$). According to theory, the occurrence of E_s is expected when the vertical zonal wind shear, which is mainly owing to solar tides, is negative. 4-year means, based on 3-monthly running mean zonal means from December 2006 - November 2010, were constructed for the terdiurnal oscillation in the occurrence frequency of E_s . Comparison of the results with VHF meteor radar observations of the terdiurnal tide and the 8-hr oscillation in the vertical zonal wind shear at Collm, Germany (51.3°N , 13°E) shows a clear correspondence between the 8-hr E_s and wind shear signature.

Zusammenfassung

Radiokultationsmessungen auf der Basis von GPS-Messungen der FORMOSA SATellite mission-3/Constellation Observing System for Meteorology, Ionosphere and Climate-Satelliten wurden verwendet, um die Signatur der 8-stündigen Gezeiten in den Auftrittsraten von sporadischen E (E_s)-Schichten zu analysieren. Nach der allgemein anerkannten Windscherungstheorie treten E_s -Schichten im Bereich negativer vertikaler Windscherung auf, welche in der unteren Thermosphäre hauptsächlich durch solare Gezeiten hervorgerufen werden. Speziell werden hier 4-jährige Mittelwerte saisonal gemittelter Auftrittsraten untersucht um die 8-stündige Signatur zu finden. Ein Vergleich mit Radarmessungen des Windes über Collm zeigt, dass die saisonale und tägliche Variabilität der 8-stündigen Komponente der E_s -Raten sehr gut mit derjenigen der gemessenen Windscherung übereinstimmt.

1 Introduction

The wind fields of the mesosphere/lower thermosphere (MLT) are strongly influenced by atmospheric solar tides. These are global waves with periods of a solar day and its subharmonics and are therefore named diurnal tide (DT), semidiurnal tide (SDT), terdiurnal tide (TDT), etc. The tides are excited by absorption of solar radiation in the lower atmospheric layers (troposphere, stratosphere) and partly by wave-wave interactions (Teitelbaum et al., 1989). The wind amplitudes are small (on the order of few cm/s) near the region of forcing, but increase significantly with height due to the decreasing air density. They maximise in the MLT at midlatitudes (Hagan et al., 1995). At these altitudes, the tides are the most dominant dynamical feature. The amplitudes are of the order of the magnitude of the mean wind and exceed those of planetary or gravity waves. Therefore, solar tides play an important role in the global circulation

and a more accurate knowledge would result in a better understanding of the dynamics in the MLT. At midlatitudes, the strongest tide is the SDT, but in October the TDT also reaches significant amplitudes of 10 m/s and more (Fytterer and Jacobi, 2011). Thus, and since the climatology of the TDT is less intensely investigated than that of the DT and SDT so far, the TDT should be considered for further investigations of the global dynamics.

Sporadic E (E_S) layers are thin clouds of enhanced electron density, at midlatitudes primarily occurring in summer. They generally form in the upper MLT (90 – 120 km), which is equivalent to the lower ionospheric E region. According to wind shear theory (Whitehead, 1961) the forming process of E_S is influenced by Earth's magnetic field, the ion concentration and the vertical wind shear as well. Neglecting diffusion, the vertical velocity of the neutral gas and the electric force, the vertical ion velocity w_{Ion} can be written as:

$$w_{Ion} = \frac{r \cdot \cos I}{I + r^2} U - \frac{\cos I \cdot \sin I}{I + r^2} V, \quad (1)$$

where U and V are the zonal and meridional wind component of the neutral gas, while I is the inclination of the Earth's magnetic field. The parameter $r = (v_{Ion/N} \cdot m_{Ion}) / (e \cdot B_0)$ includes the ion-neutral gas collision frequency $v_{Ion/N}$, the ion mass m_{Ion} , the elementary charge e and the total intensity B_0 of the Earth's magnetic field. Note that for deriving Eq. 1 Cartesian coordinates were used (x , y and z point eastward, northward and upward, respectively), which differs from the usual notations in literature. Considering that $r \gg 1$ at atmospheric regions below ~115 km (Bishop et al., 2003), the zonal wind component is significantly more efficient in causing a vertical plasma motion than the meridional wind component.

Furthermore, the formation of E_S requires negative vertical wind shear (Eq. 1), whose main source are the solar tides, partly providing larger vertical wind gradients than the background wind. Considering wind shear theory thus tidal-like structures are expected in E_S . Recent studies have shown from phase comparison of the SDT wind shear and E_S signature that the latter are most likely caused by the SDT (Arras et al., 2009). Therefore, it appears also promising to search for a relation between the TDT and terdiurnal oscillations in E_S .

In the following we analyse the terdiurnal signature in VHF meteor radar winds and wind shear over Collm, Germany. The seasonal cycle of these amplitudes will be compared against the TDT signature in E_S obtained from Global Positioning System (GPS) radio occultation (RO) measurements by the FORMOSA SATellite mission-3/Constellation Observing System for Meteorology, Ionosphere and Climate (FORMOSAT-3/COSMIC). TDT phases as seen in E_S and wind shear will be compared as well.

2 Measurements and data analysis

The GPS RO technique is used here to analyse the behaviour of E_S . The method bases on radio links between Low-Earth Orbiting (LEO) satellites and GPS satellites. We

use FORMOSAT-3/COSMIC measurements, assuring global coverage as well as a high vertical resolution. Due to the low Earth orbits of the FORMOSAT-3/COSMIC satellites, the GPS satellites are nearly fixed with respect to them and are observed as setting or rising objects. During this occultation the GPS signal is modified according to the atmospheric refraction index, containing information about air temperature, air pressure, water vapour content and electron density. The first three parameters are mainly tropospheric disturbances and are negligible in the ionosphere. As a result one occultation provides a complete vertical profile of the electron density. By analysing the signal-to-noise ratio (SNR), it is possible to extract an E_S signature from the background noise (Wu et al., 2005).

The disturbances of the signal are caused by divergence/convergence of the radio wave, leading to a decreased/increased intensity of the received signal. For analysis, first the SNR is normalised by dividing the measured SNR by the respective mean SNR. In the next step a band pass filter is used, only accepting disturbances smaller than 5 km in height range to account for the thin structure of E_S layers. Furthermore, the standard deviation of the normalised SNR is calculated for each height interval covering a sliding window of 2.5 km. Since E_S cause sharp gradients in the electron density within a few kilometres, the fluctuations have to be strong and show a sharp vertical gradient. Consequently, the standard deviation of the normalised SNR should exceed the empirically found threshold of 0.2 and rises above 0.14 between two adjacent intervals to be accepted as an E_S signature. Note that if the standard deviation rises above the limit 0.2 in more than 5 intervals, the profile is excluded from further investigations to avoid similar disturbances from other sources (Arras, 2010). The height of maximum deviation from the mean profile is regarded as the approximate altitude of the E_S . Assuming spherical geometry the E_S is located where the radio wave is most refracted (the tangent point), whose exact coordinates are calculated, using at least four GPS satellites.

The six FORMOSAT-3/COSMIC satellites are operating since summer 2006, but this study only considers zonal mean values from December 2006 – November 2010. Therefore, the ROs of every longitude in the latitude range $43^\circ\text{N} - 63^\circ\text{N}$ are used, with the mean latitude of the occultations within this interval at 51°N . The time interval includes 3 months and the reference month was taken as the second one of the interval, i.e. as the centre of the interval.

As can be seen in Fig. 1, the available data are nearly uniformly distributed among seasons, with about 10000 per month (30000 per season). Lower sample rates only occur in 2010, because satellites were out of contact or some new firmware was tested (CDAAC Team, 2012). But for constructing the climatology a sufficient amount of data still remains. To give an overview of the general characteristics of the detected E_S , Fig. 2 shows the seasonal cycles of the total number of E_S (upper panel) and of the occurrence frequency (lower panel). The latter one is the number of detected E_S divided by the respective number of ROs and finally multiplied by the factor 1000 for more handy values. Averages over a sliding height interval of 11 km, shifted by 1 km, were calculated and the reference height was taken as the centre of the interval. The above mentioned time and vertical height intervals are used in every following plot

concerning E_S , unless explicitly stated. The behaviour of E_S number and occurrence frequency is quite similar, due to the equally distributed RO in the course of a year. In general, E_S rates maximise around 105 km. In summer, more than 4500 E_S per season and 11 km interval were detected. The respective occurrence frequency reaches values above 0.14. This seasonal cycle is caused by the variations of the meteor rates (see, e.g., Haldoupis et al., 2007, their Fig. 3), in combination with the dynamics in the MLT. Significantly lower E_S rates are observed below 90 km and above 115 km, as well as from December until April.

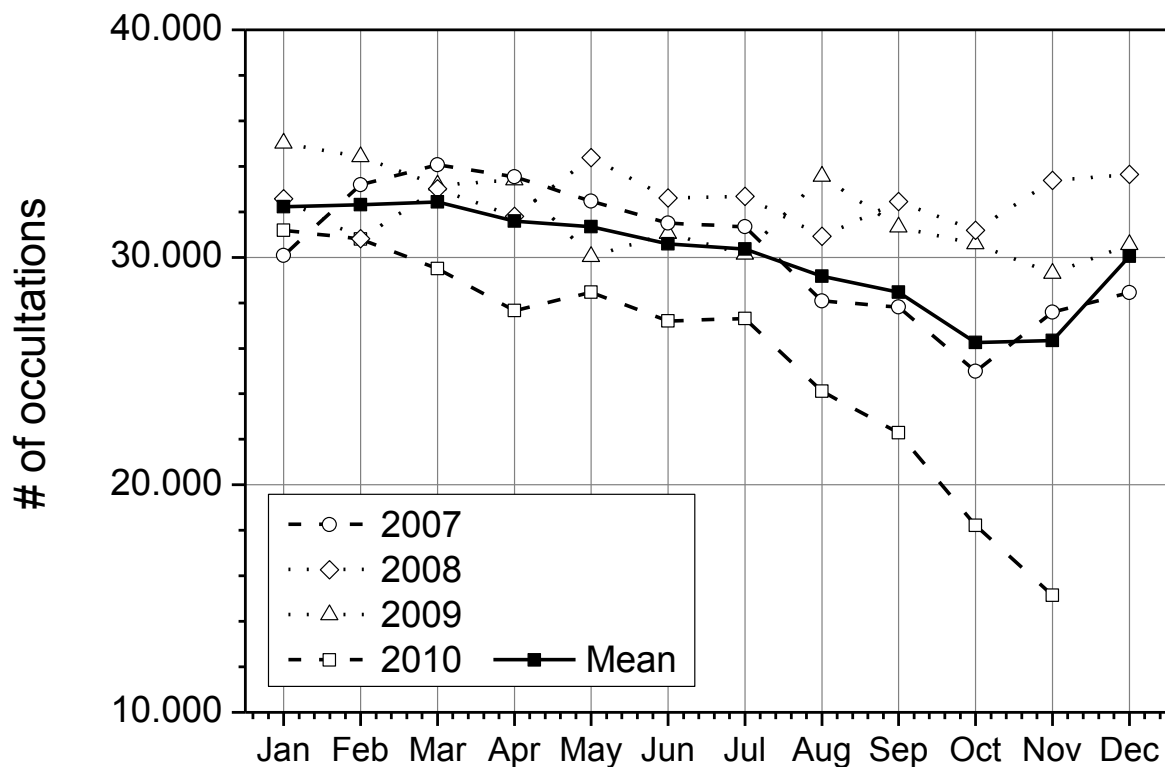


Figure 1: 3-monthly numbers of radio occultations in the latitude range $43^{\circ}\text{N} - 63^{\circ}\text{N}$ measured by the FORMOSAT-3/COSMIC satellites. The reference month represents the centre of the respective time interval. The 4-year mean (solid curve) also includes the data for December 2006, which is not shown in the figure.

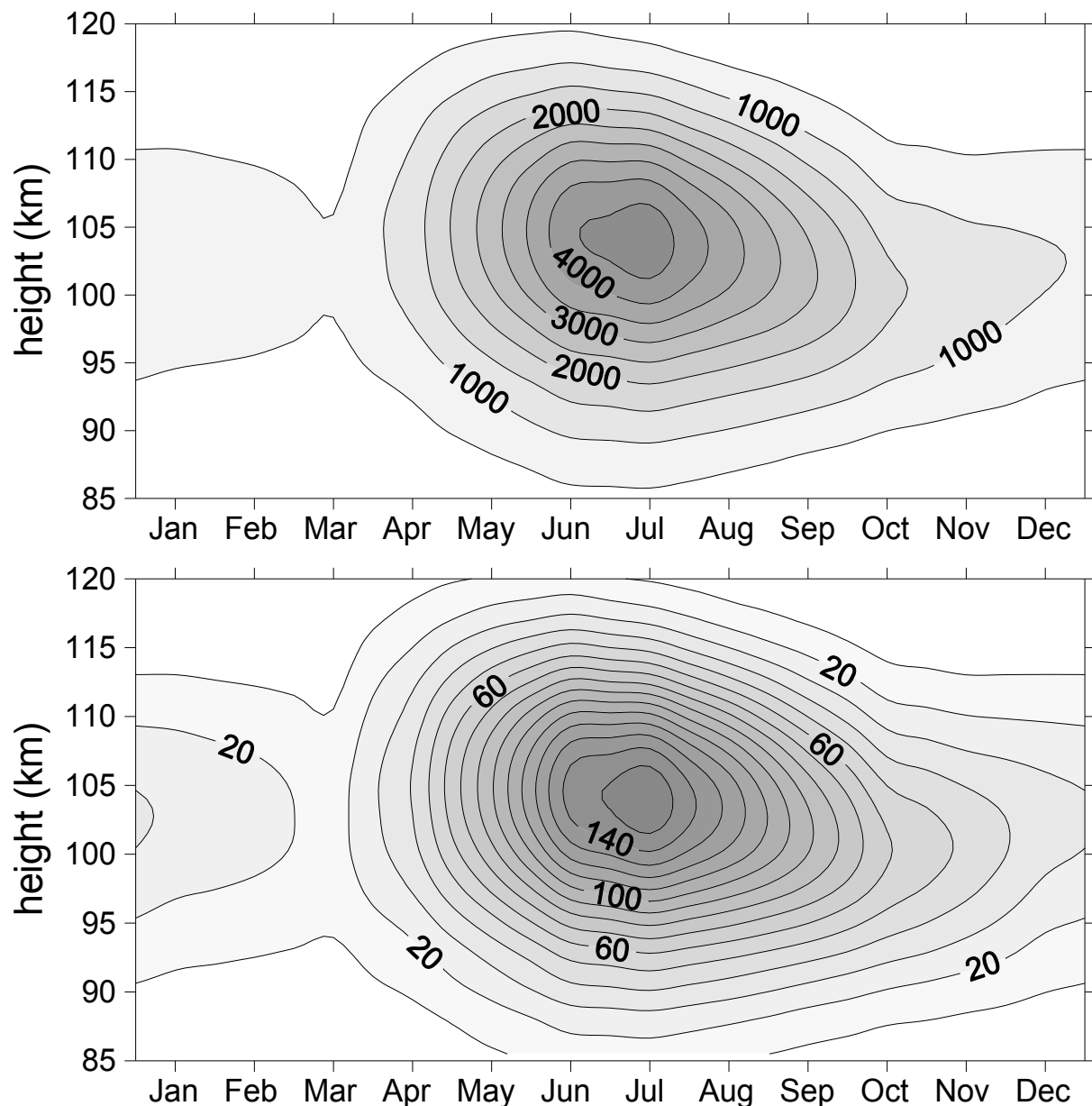


Figure 2: Seasonal cycle of the total number of sporadic E layers (upper panel) and the occurrence frequency (in 1/1000, lower panel) in the latitude range $43^{\circ}\text{N} - 63^{\circ}\text{N}$ as derived from FORMOSAT-3/COSMIC measurements. Shown are 4-year averages calculated from 3-monthly running mean zonal means using data from November 2006 – December 2010 with the respective height interval covering a sliding window of 11 km width, shifted by 1 km.

The SKiYMET meteor radar located at Collm, Germany (51.3°N , 13°E) has been in operation nearly continuously since July 2004 and the 7-year dataset from August 2004 – July 2011 is used here for analysing the vertical wind shear and the TDT. The radar is operated at 36.2 MHz with a pulse repetition frequency of 2144 Hz, a peak power of 6 kW and a pulse length of 2 km. The emitted VHF radio wave is scattered

by ionised meteor trails. The detection array includes five antennas forming an asymmetric cross to act as an interferometer. This constellation allows, in combination with range measurements, the calculation of the position of the detected meteor trail. The meteor rates vary strongly in time and space, peaking in summer and slightly below 90 km, respectively (Fig. 3). The investigated height interval is divided into six non-overlapping height gates, binned at 82, 85, 88, 91, 94 and 98 km. Note that the real mean meteor height in the uppermost gate is only 97 km due to the decreasing meteor rates with altitude (Jacobi, 2012). The radial wind velocity is obtained from the Doppler phase progression with time at each receiver. Horizontal half-hourly mean winds are calculated through projecting these mean winds on the individual radial winds and minimizing the squared differences. An outlier rejection is added (Hocking et al., 2001). Half-hourly wind shears are calculated from the difference of the winds at two adjacent height gates.

Monthly mean winds and tidal (8, 12, 24 hr) amplitudes and phases are calculated using a multiple regression analysis of the half-hourly mean winds as well as the wind shears. The procedure is described in detail in Jacobi (2012). Three-monthly running means are calculated using vector averaging for the phases and arithmetic averaging for the amplitudes.

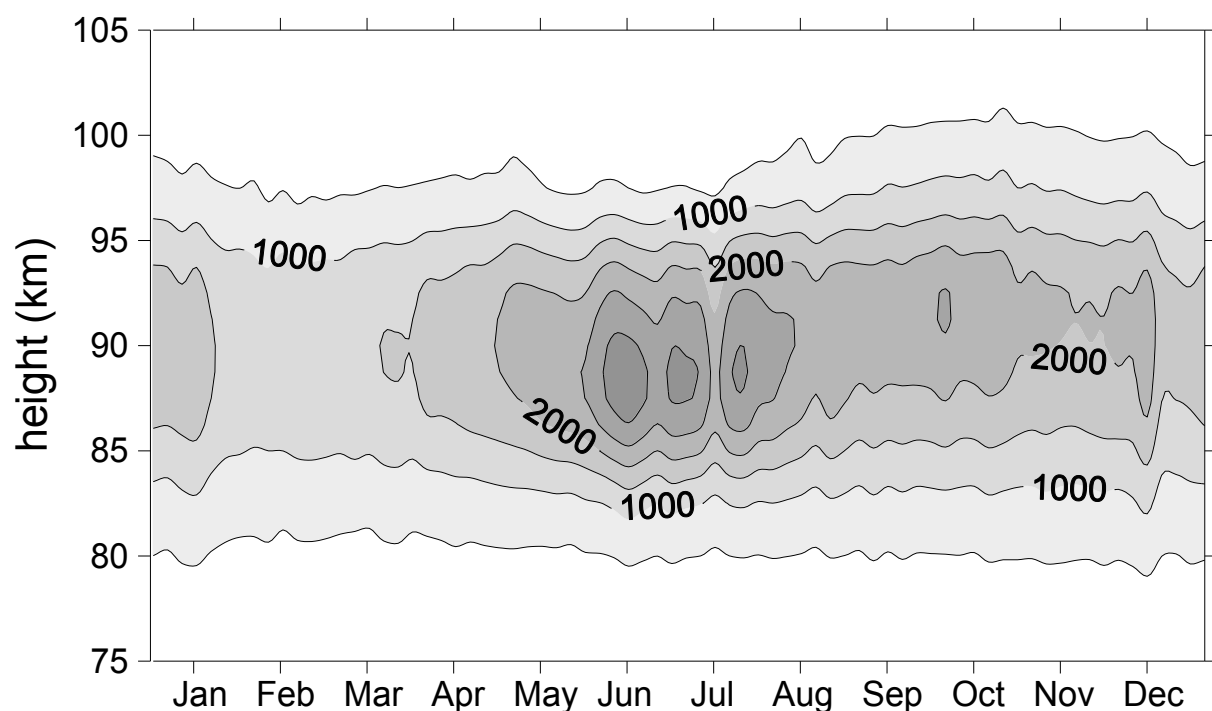


Figure 3: Height-time cross-section of 2005–2010 mean meteor count rates per day and per 5 km interval as measured by the meteor radar at Collm.

3 Results

To investigate the structure of the E_S rates in more detail, the terdiurnal oscillation was extracted from the occurrence frequency (referred here as 8-hr E_S) by using the same kind of multiple regression analysis as has been applied for the winds, but on the E_S data from each longitude, which had been sorted according to local time, while the time resolution was set to 1 hr. Previously performed frequency-wave number analyses (not shown here) have ensured that the westward migrating component is the dominant oscillation in 8-hr E_S . Each fit includes the occurrence rates during 3 months. This analysis applied for 12 data windows centred at each month of the year. The height interval covers a sliding window of 11 km, which is shifted by 1 km.

To introduce the analysis and to visualize the 8-hr oscillation in E_S , as an example, Fig. 4 (left panel) shows the 3-monthly mean hourly occurrence rates and modelled values derived through least-squares fitting of a mean, 8-hr, 12-hr, and 24-hr component (dashed line). The used harmonic fit matches well with the observed occurrence rates, indicating that no further significant oscillations are present in the diurnal cycle of the E_S rates. However, the terdiurnal wave signature is hardly visible, because the 24-hr and 12-hr waves are dominating. Therefore, the harmonic analysis was repeated here without considering an 8-hr component (solid line in Figure 4a), and the residuals are plotted in Figure 4b. Now the terdiurnal signature is clearly visible. Note that the shown fit of an 8-hr oscillation in Figure 4b provides nearly identical coefficients than the same harmonic fit applied for the original occurrence rates.

Using ionosonde measurements from July 2006 to June 2007 over Tehran, Iran (35.4°N , 51.2°E), Karami et al. (2012) also investigated 8-hr signatures in E_S . They found terdiurnal variations in the E_S critical frequency (f_0E_S) in spring and summer and in the E_S virtual height ($h'E_S$) in summer and winter, respectively. This also indicates that the terdiurnal tide-like oscillation in E_S as seen by GPS RO has a physical reason and is not a mere mathematical artefact.

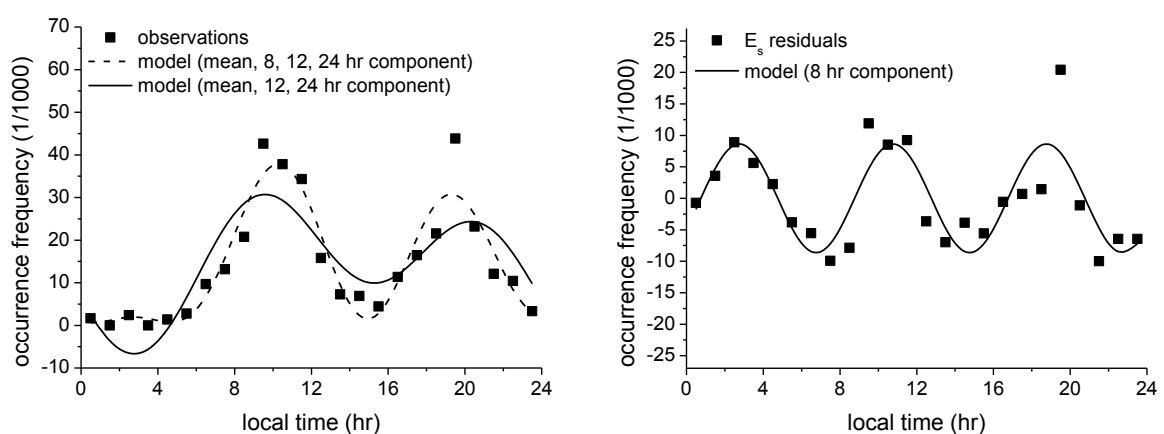


Figure 4: Comparison of the measured occurrence rates with the fitting results at ~ 112.5 km during October 2010 for a latitude range from 43°N – 63°N (left panel). The right panel shows the residuals from a fit that includes the 12 and 24-hr component and the results of fitting an 8-hr component on these.

The seasonal cycle of the amplitude of the 8-hr E_s signature, given in Fig. 5, reveals nearly no activity below 90 km and in winter, while the maximum occurs around 105 km during summer, reaching values above 0.022. The corresponding occurrence rate is about $\sim 140/1000$, revealing that 22/140 ($\sim 15\%$) of the E_s variability is caused by the 8-hr E_s . In contrast to the occurrence rates, a secondary maximum is visible in late autumn ($>10/1000$), where the 8-hr E_s influence increased to 10/40 (25%). This indicates at least one additional 8-hr signature source. Considering wind shear theory, the influence of the TDT is suggested, because the TDT reaches maximum amplitudes in autumn (Fytterer and Jacobi, 2011).

The observed seasonal behaviour is in good agreement with the results presented by Haldoupis and Pancheva (2006), who investigated terdiurnal tide-like oscillations in f_0E_s observed by the ionosonde at Rome (41.9°N , 12.5°E). Their analysed data included the years 1980 – 1991, but only the months May – October. However, the seasonal characteristics of the 8-hr E_s amplitude are strongly related to the behaviour of the occurrence frequency (Fig. 2, lower panel) and the dominating maximum in summer might be due to the higher E_s mean rates, which generally cause larger absolute fluctuations. Therefore, the influence of the background E_s activity cannot be neglected and has to be taken into account in further analysis.

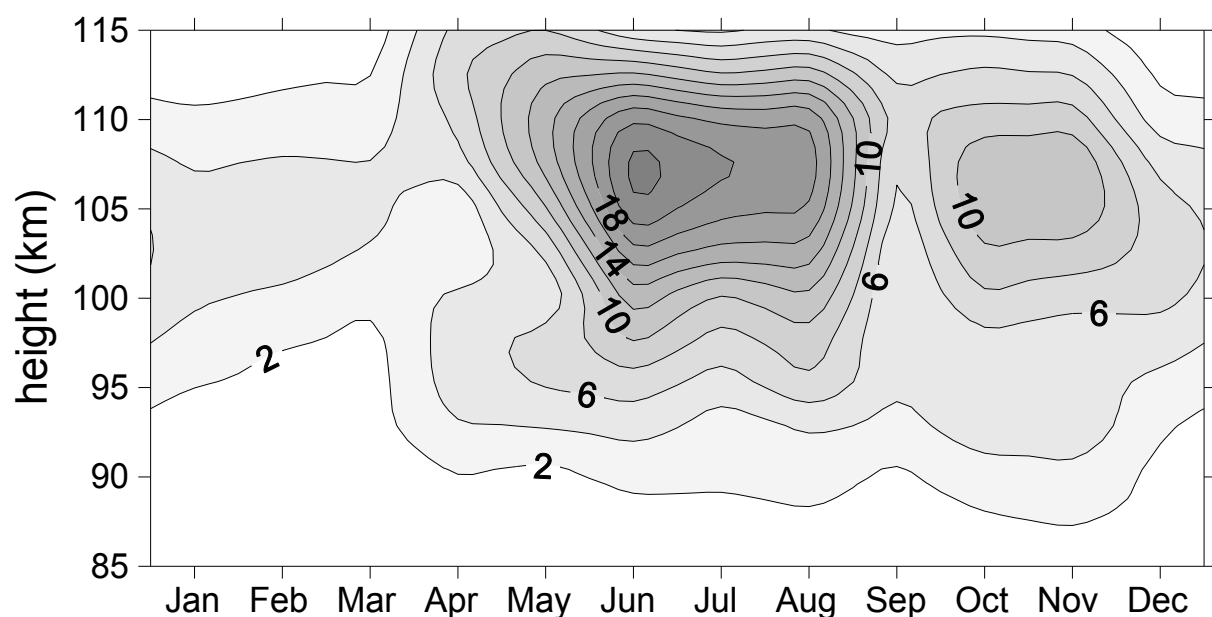


Figure 5: Amplitude (given in 1/1000) of the 8-hr oscillation within the occurrence frequency of the sporadic E layers.

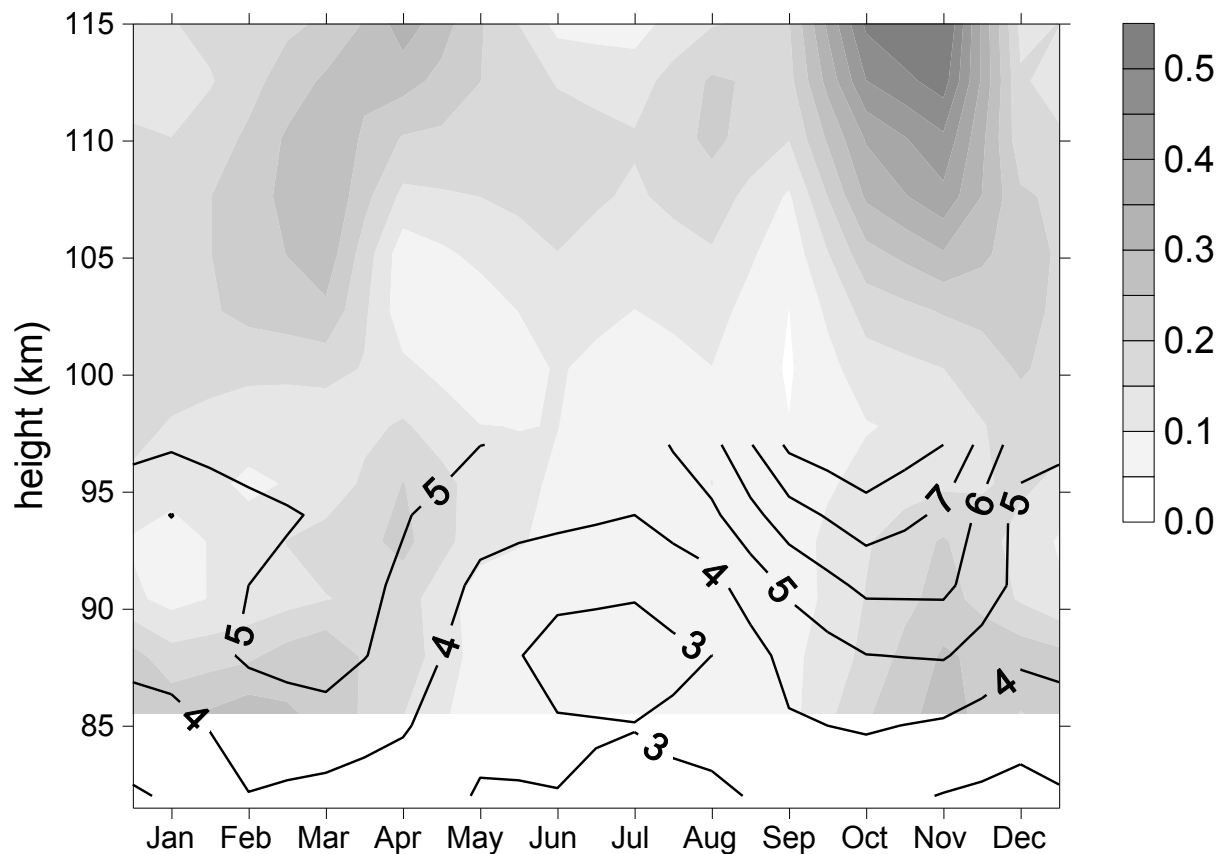


Figure 6: Normalised amplitude of the 8-hr oscillation within the E_s occurrence frequency (grey shading). Isolines show the amplitude (m/s) of the terdiurnal zonal wind tide, measured by the meteor radar at Collm, using the data from August 2004 – July 2011.

The amplitudes of the 8-hr E_s were normalised by dividing them through the respective 3-monthly mean zonal mean E_s occurrence rates. The results are presented in Fig. 6 (grey shading) and were compared with the amplitude of the TDT as observed by meteor radar (isolines). The obtained normalised amplitudes do not show maximum values in summer any more, confirming wind shear theory as 8-hr signature source. The largest values are seen in October and November, reaching amplitudes of ~ 0.5 between 110 km and 115 km. Also evident is a secondary maximum in spring, which is weaker by a factor of 2. This seasonal cycle closely correlates with the one of the wind TDT at lower heights, where the amplitudes are also small during summer ($\sim 3 - 4$ m/s) and maximise in October (~ 8 m/s) and March (~ 5 m/s), respectively. Note that the TDT wind amplitudes generally increase with height, while the 8-hr E_s amplitude decreases between 90 km and 100 km, in particular during equinoxes. This may be due to the low E_s rates (see Fig. 2) and the weak absolute amplitudes (Fig. 5), which means that small fluctuations can result in strong relative variations. This behaviour is not seen in summer. Furthermore, the maxima in both seasonal cycles are slightly shifted in time. However, a full agreement cannot be expected, due to the different observed height intervals.

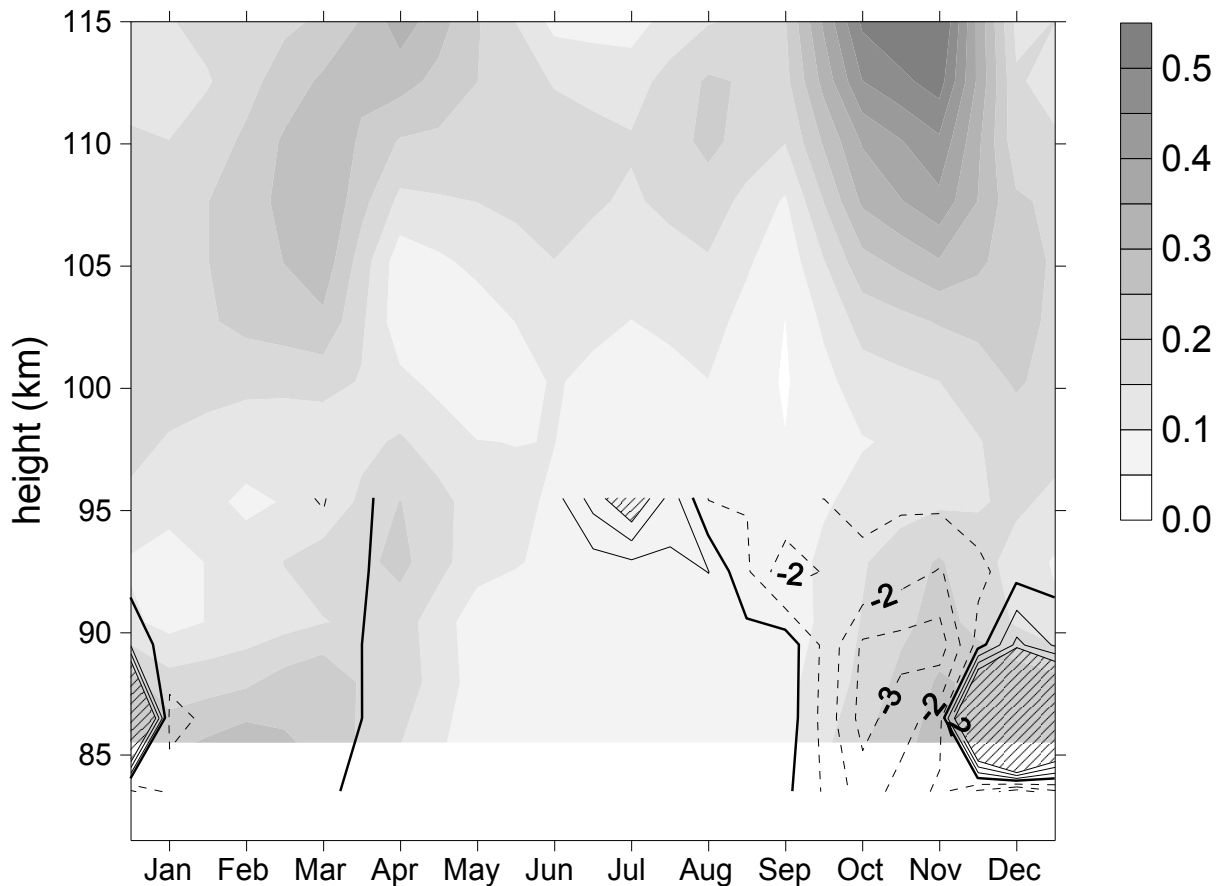


Figure 7: Normalised amplitude of the 8-hr oscillation within the occurrence frequency of the sporadic E layers (grey shading). The isolines show the normalised amplitude of the 8-hr oscillation in the vertical wind shear, as measured by the meteor radar at Collm, using the data from August 2004 – July 2011. The zero wind shear line is highlighted and negative shear values are marked as dashed isolines.

Assuming that E_S are formed by the wind shear mechanism, the 8-hr oscillation in the vertical wind shear (referred to as 8-hr shear here) was calculated and subsequently normalised by dividing the 8-hr shear amplitude by the respective mean shear. In Fig. 7, the normalised 8-hr shear is compared with the normalised 8-hr E_S amplitude. Note that the mean shear is sometimes very low, which leads to large normalised values (dashed areas), which should not be over-interpreted. Large negative values, which are observed in autumn (~ -3), imply a negative mean shear together with comparatively large 8-hr shear amplitudes. In general, negative normalised amplitudes dominate from September through March, while positive ones are present in summer and late spring. This correlates with the seasonal behaviour of normalised 8-hr E_S as well as the amplitude of the TDT. Note that the result corresponds to the wind shear theory, because during positive mean wind shear, tides can still provide a negative shear gradient.

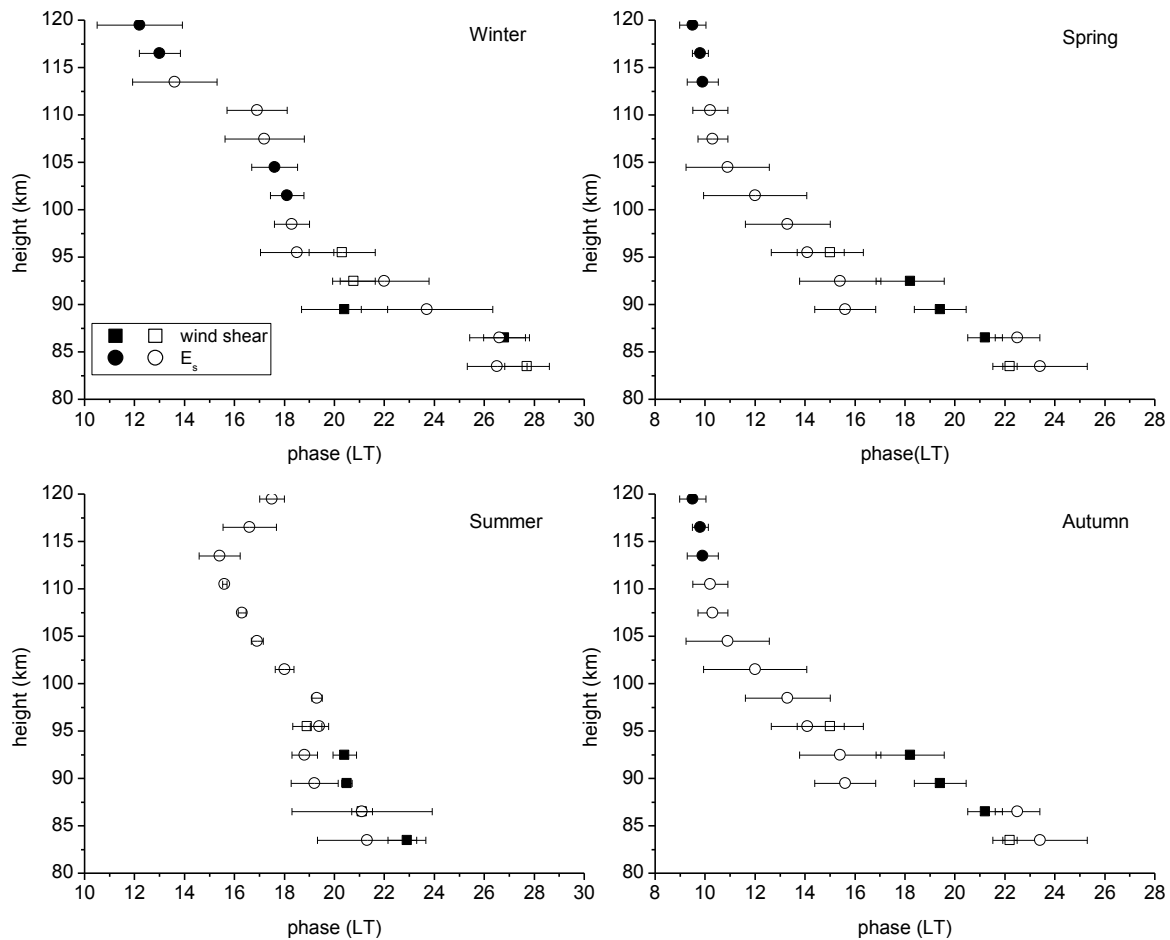


Figure 8: Phases of the 8-hr oscillations in the zonal vertical wind shear (squares) and the sporadic E layers (circles) for each season, based on 3-monthly running means from January 2007 – October 2010. Solid symbols indicate significant amplitudes according to a t-test. The error bars indicate the standard deviation of the individual seasonal mean values.

To further confirm the relation between the wind shear and the occurrence rates of E_S , Fig. 8 shows the phases of the 8-hr wind shear (squares) and the 8-hr E_S (circles). Note that the latter one is defined as the local time of maximum E_S probability, while the 8-hr shear phase is given as the time of maximum negative wind shear. The seasonal means from 2007 – 2010 were vector averaged and the standard deviation (shown as error bars) was calculated from the 4 years of seasonal mean data, thereby indicating interannual variability. This was carried out for each 7 km height interval, using a 3 km overlap. The reference height was taken as the centre of the interval. Significant phases (solid symbols) of the 8-hr shear generally occur between 86.5 km and 92.5 km, except for winter. In summer and autumn, also the lowest or uppermost gates, respectively, show significant values. In contrast to that, the 8-hr E_S phases reveal only a few significant values, which were observed around 113 km in spring and slightly above 100 km during winter. However, in autumn, significant values are al-

ways present in the height interval 100 – 113 km, suggesting the influence of the wind shear TDT on E_S .

Generally, the 8-hr E_S phases show the descent of the E_S layer with time. This is according to theory (Haldoupis et al., 2006), where E_S layers follow the phase velocity of the tides, but this is the case only above 100 km. In lower regions they slow down, due to the increasing ion-neutral gas collision frequency. A tendency for this can be seen in spring and summer, where the E_S phase is slightly bent around 100 km. A bending in autumn and winter is also weakly indicated, but it is, as is seen by the large error bars, not a regular feature. There are two reasons for these observations. On the one hand the GPS RO technique is not able to track a single E_S . Consequently, fine-scale characteristics like the bending can only be seen in spring and summer, when a sufficient amount of E_S data is available. Furthermore, at lower altitudes (<100 km) some phase shifts occur, e.g., in autumn 2010 at ~90 km (not shown here), or generally in spring at ~90-95 km resulting in strong differences with respect to the expected values. Note that those described phase shifts are evident in E_S and wind shear data.

The vertical wavelength of the 8-hr shear is short during spring (excluding the uppermost gate) and summer, but significantly longer during autumn and winter. This correlates with the behaviour of the TDT phases. However, the vertical wavelength of the TDT in E_S or wind shear is also dependent of the amplitude change with height therefore cannot be directly compared with the wind amplitude phase gradient.

Although the majority of measured 8-hr E_S amplitudes are insignificant, the general correspondence between the phases of 8-hr shear and 8-hr E_S gives additional confidence that we observed a real phenomenon and not an artefact. The closest agreement between the phase profiles is seen in summer, although the TDT activity is low. In contrast, during autumn the agreement is less strong, while the TDT amplitudes are large. In spring and summer, an overlapping between the phase profiles was observed, and the extrapolated 8-hr shear phases fit well with the 8-hr E_S phases in higher altitudes. Again, this is caused by the decreasing E_S rates below 100 km and the fact that the E_S phases are less strongly determined by the phases of the tides in these regions. Lower E_S rates are also a reason for the phase shifts in some altitudes.

4 Conclusions

The terdiurnal oscillations in the occurrence frequency of E_S were analysed based on the measurements of the FORMOSAT-3/COSMIC satellites. The performed GPS RO technique does not allow tracking of a single E_S , but information about the seasonal characteristics are available. Therefore, the 3-monthly running mean zonal means from December 2006 – November 2010 were used for constructing 4-year means. After removing the effect of the background E_S activity, we found that the seasonal cycle of the normalised amplitude of the 8-hr E_S is marked by two maxima during spring and autumn, while the latter one is dominating. This agrees well with the seasonal behaviour of the 8-hr amplitudes in wind and wind shear, which gives a strong indication for close physical connection between E_S and the TDT. We could also show that the 8-hr shear phases match the 8-hr E_S phases, which is the case especially when the E_S rates

are high. Therefore, the 8-hr E_S is also forced or at least significantly influenced by dynamics. Furthermore the clearest signature of the 8-hr shear is observed in autumn, correlating with the stronger TDT activity.

These qualitative correlations between the 8-hr signatures in E_S and wind/wind shear were not expected, because the 8-hr E_S oscillations based on zonal means, while the radar measurements of the wind field over Collm are affected by local phenomena. Therefore the results indicate that, according to wind shear theory, besides the well-known influence of the SDT also the TDT plays a role in the diurnal and seasonal cycle of E_S .

Acknowledgements

This study was supported by Deutsche Forschungsgemeinschaft under grant JA 836/22-1. We acknowledge UCAR (Boulder, U.S.) and NSPO (Taiwan) for the free provision of FORMOSAT-3/COSMIC data and related support. We also thank Falk Kaiser, Leipzig, for maintaining the radar measurements.

References

- Arras, C., 2010: A global survey of sporadic E layers based on GPS Radio occultations by CHAMP, GRACE and FORMOSAT-3 / COSMIC. PhD thesis, University of Leipzig, 127 p.
- Arras, C. Jacobi, C., Wickert, J., 2009: Semidiurnal tidal signatures in sporadic E occurrence rates derived from GPS radio occultation measurements at higher midlatitudes. *Ann. Geophys.*, 27, 2555–2563.
- Bishop, R.L., Earle, G.D., 2003: Metallic ion transport associated with midlatitude intermediate layer development. *J. Geophys. Res.*, 108, A11019, doi:10.1029/2002JA009411.
- CDAAC Team, 2012: <http://cdaac-www.cosmic.ucar.edu/cdaac/status.html>, last access: 26 June 2012.
- Fytterer, T., Jacobi, C., 2011: Climatology of the 8-hour tide over Collm (51.3°N, 13°E). *Rep. Inst. Meteorol. Univ. Leipzig*, 48, 23-32.
- Hagan, M.E., Forbes, J.M., Vial, J., 1995: On modeling migrating solar tides. *Geophys. Res. Lett.*, 22, 893–896.
- Haldoupis, C., Pancheva, D., 2006: Terdiurnal tidelike variability in sporadic E layers. *J. Geophys. Res.*, 111, A07303, doi:10.1029/2005JA011522.
- Haldoupis, C., Meek, C., Christakis, N., Pancheva, D., Bourdillon, A., 2006: Ionogram height-time-intensity observations of descending sporadic E layers at mid-latitude. *J. Atmos. Sol.-Terr. Phys.*, 68, 539-557, doi:10.1016/j.jastp.2005.03.020.

Haldoupis, C., Pancheva, D., Singer, W., Meek, C., MacDougall, J., 2007: An explanation for the seasonal dependence of midlatitude sporadic E Layers. *J. Geophys. Res.*, 112, A06315, doi:10.1029/2007JA012322.

Hocking, W.K., Fuller, B., Vandeppeer, B., 2001: Real-time determination of meteor-related parameters utilizing modern digital technology. *J. Atmos. Sol.-Terr. Phys.*, 63, 155–169.

Jacobi, Ch., 2012: 6 year mean prevailing winds and tides measured by VHF meteor radar over Collm (51.3°N, 13.0°E). *J. Atmos. Sol.-Terr. Phys.*, 78-79, 8-18, doi:10.1016/j.jasp.2011.04.010.

Karami, K., Ghader, S., Bidokhti, A.A., Joghataei, M., Neyestani, A., Mohammadbadi, A., 2012: Planetary and tidal wave-type oscillations in the ionospheric sporadic E layers over Tehran region. *J. Geophys. Res.*, 117, A04313, doi:10.1029/2011JA017466.

Teitelbaum, H., Vial, F., Manson, A.H., Giraldez, R., Massebeuf, M., 1989: Non-linear interactions between the diurnal and semidiurnal tides: terdiurnal and diurnal secondary waves. *J. Atmos. Sol.-Terr. Phys.*, 51, 627–634.

Whitehead, J., 1961: The formation of the sporadic E layer in the temperate zones. *J. Atmos. Terr. Phys.*, 20, 49-58.

Wu, D.L., Ao, C.O., Hajj, G.A., de la Torre Juarez, M., Mannucci, A.J., 2005: Sporadic E morphology from GPS-CHAMP radio occultation. *J. Geophys. Res.*, 110, A01306, doi: 10.1029/2004JA010701.

Addresses of Authors

Tilo Fytterer: Now at Karlsruhe Institute of Technology, Institute for Meteorology and Climate Research

Christina Arras: German Research Centre for Geosciences GFZ, Potsdam, Department Geodesy & Remote Sensing, Telegrafenberg, 14473 Potsdam

Christoph Jacobi: Institute for Meteorology, Universität Leipzig, Stephanstr. 3, 04103 Leipzig